

# **Abstract**



# Acknowledgements



# Contents

<b>1</b>	<b>Introduction</b>	<b>7</b>
<b>2</b>	<b>Theory</b>	<b>9</b>
2.1	Spin-orbit coupling . . . . .	9
2.2	Wannier Functions . . . . .	9
<b>3</b>	<b>Charge order and spin-momentum locking in high spin-orbit coupled ferroelectrics</b>	<b>11</b>
3.1	Introduction . . . . .	11
3.2	Rashba-Bychkov Effect . . . . .	12
3.3	Orbital Rashba Effect . . . . .	13
3.3.1	Tight-Binding model . . . . .	14
3.4	Overview: Germanium Telluride . . . . .	16
3.5	Band structure . . . . .	16
3.6	Methods . . . . .	18
3.7	Results and Discussion . . . . .	19
3.8	Conclusions . . . . .	20



# **Chapter 1**

# **Introduction**



# Chapter 2

## Theory

### 2.1 Spin-orbit coupling

### 2.2 Wannier Functions

In a lot of the work presented in this Thesis we construct models to describe the physics that result in a certain effect in real materials. These models are most of the time defined in terms of a limited set of local atomic-like orbitals, since these offer the most intuitive understanding most of the time, and the biggest contribution to particular effects can often be traced back to only a limited subset of all the orbitals.

If we want to apply these models to real materials to get not only qualitative, but also quantitative results, we need to perform a fit to either experimentally obtained values, or first-principles simulations. The most feasible way is usually the latter, which requires us to find a bridge between the plane waves that are used in a lot of first-principles DFT codes, and the localized basis set of that the model is built from.

Wannier functions offer a rigorous and flexible solution to this question, rewriting the Bloch functions as a discrete Fourier transform of (exponentially) localized, cell-periodic wavefunctions.

This construction is flexible in the sense that it is not unique. Bloch functions have a gauge freedom at each  $k$  value, which in turn will have an effect on the Wannier functions. One gauge that is commonly used is the one that localized the functions as much as possible, leading to the so-called Maximally Localized Wannier Functions (MLWF). Other gauges can be chosen such that the obtained functions have certain symmetries or have maximum similarity to atomic orbitals.



# Chapter 3

## Charge order and spin-momentum locking in high spin-orbit coupled ferroelectrics

### 3.1 Introduction

The research area of spintronics aims to supersede electronics by using spins instead of charges for information processing and storage. Many possible devices that utilize both charge and spin degrees of freedom of carriers have been theorized. Examples are the spin field-effect transistors (spin-FET) Datta and Das (1990), storage devices which utilize spin-current and associated spin-transfer torque to efficiently manipulate magnetic domains Kent and Worledge (2015); Jungwirth *et al.* (2016). In spite of fundamental interest and potential for applications, the actual realization of these devices has been rather elusive. One of the main culprits for the limited success to date is that the devices require very granular, ideally electric, control of the spin, which is impeded by widely separated energy scales and weak coupling between magnetic and structural degrees of freedom. One class of materials that allow for such electric control of spin-polarized states are the ferroelectric semiconductors with large atomic spin-orbit coupling (SOC) Di Sante *et al.* (2013); Ishizaka (2011); Kim *et al.* (2014). The underlying mechanism is a coupling between the spin-polarized states and the ferroelectric polarization of the material that makes it possible to switch the ferroelectric polarization and in turn the polarization of the spin by the external electric field. The effect has been confirmed both experimentally Ishizaka (2011); Liebmann *et al.* (2016); Krempaský, *et al.* (2016), and through ab initio density functional theory (DFT) simulations Di Sante *et al.* (2013).

### 3.2 Rashba-Bychkov Effect

The first effect that springs to mind bearing the signatures of the above description is the Rashba effect, first theorised in the seminal 1959 paper by Rashba and Bychkov Rashba and Sheka (1959). This effect is a text book case where the breaking of a symmetry, in this case inversion symmetry, leads to previously degenerate states becoming nondegenerate with a definite value of the parameter describing the symmetry. In the case of the Rashba-effect, the absence of inversion symmetry leads to a breaking of the up-down symmetry of the spin of bloch functions, leading to states with definite spin polarization. These could then in turn theoretically be used in spintronics applications. We will first describe how the effect was first derived and then discuss the issues with explaining the observed spin-splitting of bloch wavefunctions in bulk ferroelectrics, and give a hint why the largest spin-polarizing effect might actually be coming from a completely different origin.

The standard derivation starts from an expansion of the electron part of the fully relativistic Dirac-equation up to second order in  $1/c$  where  $c$  is the speed of light Rashba and Sheka (1959), in the absense of an external magnetic field:

$$\mathcal{H}\psi = \left[ \frac{\mathbf{p}^2}{2m} - eV - \frac{e\hbar}{4m^2c^2}(\boldsymbol{\sigma} \cdot [\nabla V \times \mathbf{p}]) - \frac{\hbar^2}{8m^2c^2}\Delta V - \frac{\mathbf{p}^4}{8m^3c^2} \right] \psi = E\psi \quad (3.1)$$

where  $\psi$  is a two component spinor,  $V$  denotes the electric potential,  $\boldsymbol{\sigma}$  a vector of Pauli-matrices ( $\sigma_x, \sigma_y, \sigma_z$ ),  $m$  and  $e$  the electron mass and charge respectively, and  $\mathbf{p}$  the canonical momentum. The first two terms are the non-relativistic part of the Hamiltonian, the third represents the spin-orbit coupling (SOC), the fourth is known as the Darwin effect and the fifth is the relativistic correction to the effective electron mass. For the further discussion, we focus on the first three terms.

The next step is to apply the Hamiltonian to Bloch spinor wavefunctions  $\psi_n(\mathbf{k}, \mathbf{r}) = u_n(\mathbf{k}, \mathbf{r})e^{i\mathbf{k} \cdot \mathbf{r}}$ , where  $u_n$  denotes the cell-periodic part, and  $n$  is the band index. This leads to an eigenvalue equation for  $u_n(\mathbf{k}, \mathbf{r})$

$$E_n u_n(\mathbf{k}, \mathbf{r}) = (V_0 + V_1 - (V_2 + V_3)) u_n(\mathbf{k}, \mathbf{r}) \quad (3.2)$$

$$V_0 = \frac{\mathbf{p}^2}{2m} - eV + \frac{\hbar^2 k^2}{2m} \quad (3.3)$$

$$V_1 = \hbar \frac{\mathbf{k} \cdot \mathbf{p}}{m} \quad (3.4)$$

$$V_2 = \frac{e\hbar^2}{4m^2c^2} \boldsymbol{\sigma} \cdot (\nabla V \times \mathbf{k}) \quad (3.5)$$

$$V_3 = \frac{e\hbar}{4m^2c^2} \boldsymbol{\sigma} \cdot (\nabla V \times \mathbf{p}) \quad (3.6)$$

$$(3.7)$$

In the following we assume that this equation can be solved for a time reversal symmetric point  $\mathbf{k}_0$  in the first BZ, where the spin-up and spin-down part of the spinor are necessarily degenerate, and proceed following standard  $\mathbf{k} \cdot \mathbf{p}$  theory to perform an expansion around this k-point. Since including the relativistic terms

and nonzero  $\mathbf{k}$  will lead to spin up-down symmetry breaking, we will denote the down spin state as  $|u_n^\downarrow\rangle$  and up spin state as  $|u_n^\uparrow\rangle$  at  $\mathbf{k} = \mathbf{k}_0$ . We only investigate terms in the expansion that are linear in  $\mathbf{k}$ , since that's the part of the energy dispersion that we are seeking to explain. We again keep terms up to second order in  $(1/c)^{-1}$ . Without loss of generality we can take  $\mathbf{k}_0 = 0$  and  $E_0 = 0$ .

$$E_n^{\sigma_1}(\mathbf{k}) = -\langle u_n^{\sigma_1} | V_2 | u_n^{\sigma_1} \rangle + \quad (3.8)$$

$$\sum_{m,\sigma_2=\uparrow,\downarrow} \frac{\langle u_n^{\sigma_1} | V_1 | u_m^{\sigma_2} \rangle \langle u_m^{\sigma_2} | V_3 | u_n^{\sigma_1} \rangle + h.c.}{E_m^{\sigma_2} - E_n^{\sigma_1}}, \quad (3.9)$$

where the sum over  $m, \sigma_2$  includes all states which are not equal to  $n, \sigma_1$ .

These two terms are of similar order of magnitude in small parameters  $c^{-2}$  and  $\mathbf{k}$ , but have different behavior with respect to the symmetries of the states, and different origins with respect to the ferroelectricity. The first term can be seen as a direct result of the electric field resulting from the ferroelectricity, i.e.  $\nabla V$  there should be understood as the uniform internal electric field, whereas in the second term the  $\nabla V$  should be understood as the potential which causes atomic spin-orbit coupling. This means that it is important that the orbitals  $u_n$ , and  $u_m$  in the second term originate from an atom with strong spin-orbit coupling. The reason why this term only leads to a non-zero contribution when inversion is broken can be understood by looking at the required symmetries of orbitals  $u_n, u_m$ , as was shown by [Blugel paper]. Since  $\mathbf{p}$  is odd in spatial coordinates,  $\mathbf{k} \cdot \mathbf{p}$  is only non-zero when one of the orbitals is odd with respect to a spatial direction and the other even. One example could be a  $p_y$  orbital and a  $s-p_z$  hybridized one, which would be created by the ferroelectricity with electric polarization along the  $z$ -axis (add drawing? add hopping matrix?).

With regards to the size of the effect, the first term usually results in a tiny splitting, due to the tiny prefactor ( $10^{-6}$ ) and small  $\mathbf{k}$  value. The second term can be larger, because atomic SOC can be large for heavier atoms. There is, however, another possible source of spin splitting, originating from the so-called orbital Rashba effect (ORE).

### 3.3 Orbital Rashba Effect

Contrary to the relativistic effect, this one originates from electrostatic considerations. Namely, it can be shown that Bloch functions with nonzero orbital angular momentum have nonzero dipoles. This leads to two separate effects, firstly, when spin orbit coupling is included, OAM is unquenched at the high symmetry k-points, and as will be shown below, this leads to a correction to the band dispersion that varies linearly with  $\mathbf{k}$ . Secondly, this causes a linear variation of the OAM of the Bloch functions as one moves away from the high-symmetry point. If one then includes  $\mathbf{l} \cdot \boldsymbol{\sigma}$  this linear  $\mathbf{l}$  will lead to an energy contribution with either positive or negative slope. To understand this contribution, we first need to understand the behavior of the orbital angular momentum of the Bloch functions in reciprocal space. This has been first described by Park et al Park *et al.* (2011), and we will give a short derivation here.

The crux is that Bloch functions with periodic part  $u_n(\mathbf{k}, \mathbf{r})$  that have non-zero orbital angular momentum (OAM) create inter unit cell dipoles, which

couple to the uniform electric field caused by the polarization. This will thus lead to the creation of orbitals with OAM away from high symmetry points, if symmetries allow for it and ferroelectricity is present. This effect is purely electrostatic and thus doesn't come with small prefactors like the first term in ??.

### 3.3.1 Tight-Binding model

Due to the breaking of inversion symmetry there are extra allowed hopping terms between unit cells, on top of the usual ones from overlap integrals. These terms originate from the energy  $H_{isb} = e(\mathbf{d} \cdot \mathbf{E})$ , i.e. electric dipole moments coupling to the electric field. In the following we study a toy 2D square layer with one atom per unit cell and  $s, p$  orbitals, where the field is chosen perpendicular to the 2D layer along the  $z$  direction. Assuming Wannier functions  $p_\alpha(\mathbf{r}, \mathbf{R}) = \alpha e^{-|\mathbf{r}-\mathbf{R}|^2}$ , we can write down the dipole matrix terms between the central unit cell and one shifted by  $\mathbf{R} = \mathbf{n}a$ ,  $\mathbf{n} = (n_x, n_y)$  as follows:

$$\hat{d}_z(\mathbf{n}) = ae^{-\frac{a^2|\mathbf{n}|^2}{2}} \frac{\pi^{\frac{3}{2}}}{16\sqrt{2}} \begin{pmatrix} 0 & 0 & 0 & 2 \\ 0 & 0 & 0 & n_x \\ 0 & 0 & 0 & n_y \\ 2 & n_x & n_y & 0 \end{pmatrix} \quad (3.10)$$

$$= d_z^0(\mathbf{n}) \hat{d}_z^1(\mathbf{n}), \quad (3.11)$$

where the indices run through  $s, p_{x,y,z}$ . Using these Wannier functions we can write down the dipoles of Bloch functions as,

$$d_z(\mathbf{k}) = \sum_{\mathbf{n}} e^{i\mathbf{k} \cdot \mathbf{n}} d_z(\mathbf{n}) \quad (3.12)$$

$$= \sum_{\mathbf{n}} i \sin(\mathbf{k} \cdot \mathbf{n}) d_z(\mathbf{n}) \quad (3.13)$$

writing  $\mathbf{k}$  in terms of crystalline coordinates, and we kept only the  $\sin(\mathbf{k} \cdot \mathbf{n})$  part of the exponent since the  $\cos(\mathbf{k} \cdot \mathbf{n})$  part is 0 due to the fact that it is even in the sum over  $\mathbf{n} = \{-\infty, \infty\}$ , whereas  $d_z(\mathbf{n})$  is odd. If we then assume that at  $k = 0$  the Bloch functions are formed purely from these  $s, p_{x,y,z}$  Wannier functions:  $|\alpha(\mathbf{k} = 0)\rangle = \sum_{\mathbf{n}} |\alpha(\mathbf{n})\rangle$ , we can write down a perturbation theory for small  $\mathbf{k}$  in the spirit of the usual  $\mathbf{k} \cdot \mathbf{p}$  theory,

$$|\alpha(\mathbf{k})\rangle = |\alpha\rangle + \sum_{\beta} \frac{\langle \alpha | H_0(\mathbf{k}) + H_{isb}(\mathbf{k}) | \beta \rangle}{E_{\beta} - E_{\alpha}} |\beta\rangle \quad (3.14)$$

$$= |\alpha\rangle + \sum_{\beta} \frac{\langle \alpha | H_0(\mathbf{k}) + eE_z d_z(\mathbf{k}) | \beta \rangle}{E_{\beta} - E_{\alpha}} |\beta\rangle. \quad (3.15)$$

The effect of  $H_{isb}$  is to mix  $p_{x,y}$  and  $p_z$  orbitals, e.g. if  $|\alpha\rangle = p_x$  we get that

$$|\alpha(\mathbf{k})\rangle = |p_x\rangle + i \frac{eE_z \sum_{\mathbf{n}} \sin(k_x n_x) n_x d_z^0(\mathbf{n})}{E_{p_z} - E_{p_x}} |p_z\rangle \quad (3.16)$$

$$= |p_x\rangle + i c(k_x) |p_z\rangle. \quad (3.17)$$

With  $l_y = -i\hbar(z\partial_x - x\partial_z)$  we get that

$$\langle \alpha(\mathbf{k}) | l_y | \alpha(\mathbf{k}) \rangle = c(k_x) = k_x \frac{eE_z \sum_{\mathbf{n}} n_x^2 d_z^0(\mathbf{n})}{E_{p_z} - E_{p_x}} \quad (3.18)$$

**[normalization!!]** A similar term exists for  $l_x$ , but with the opposite sign. If the atomic spin-orbit coupling,  $\lambda \mathbf{l} \cdot \boldsymbol{\sigma}$ , is then taken into account, we get to a contribution to the energy dispersion  $\varepsilon(\mathbf{k}) \propto E_z(k_x \sigma_y - k_y \sigma_x)$  which has exactly the form of a Rashba splitting. This shows that the inversion symmetry breaking term will lead to a linear variation of the orbital angular momentum. When the orbitals originate from an atom with non-negligible atomic spin-orbit coupling, this linear variation of the OAM will lead to a contribution to the dispersion that varies linearly with  $\mathbf{k}$ , either upwards or downwards depending on the sign of  $\sigma$ . Except for the atomic spin-orbit coupling, which can be large, this effect is purely based around electrostatic considerations and thus does not suffer from the same minuscule prefactor as the purely relativistic Rashba effect.

This assumes that the states at the high symmetry point ( $|k| = 0$ ) have a fully quenched OAM, however, when spin-orbit coupling is included, this is only partially true. Due to the energy contribution from  $H_{soc}$  the material can gain by creating orbitals that have  $\mathbf{j} = \mathbf{l} + \boldsymbol{\sigma}$ . Similar to the above derivation, we can look at a small- $k$  expansion for orbitals that have nonzero OAM.

We can write in general that

$$\langle \alpha | \hat{l}_\gamma | \beta \rangle = i\epsilon_{\alpha\beta\gamma} c_\alpha^* c_\beta \quad (3.19)$$

when  $\alpha, \beta, \gamma$  designate  $p_{x,y,z}$ . This means that there has to be at least some admixing of multiple  $p$ -orbitals to get nonzero OAM. This leads to the following expansion of the Bloch functions around the high-symmetry  $|k| = 0$  point:

$$|\psi_n(\mathbf{k})\rangle = \sum_{\mathbf{n}, \alpha} c_\alpha(\mathbf{k}) e^{i\mathbf{k} \cdot \mathbf{n}} |\alpha(\mathbf{n})\rangle \quad (3.20)$$

$$= \sum_{\mathbf{n}, \alpha} \left( c_\alpha(0) + \mathbf{k} \frac{\partial c_\alpha(\mathbf{k})}{\partial k} \Big|_{\mathbf{k}=0} \right) (1 + i\mathbf{k} \cdot \mathbf{n}) |\alpha(\mathbf{n})\rangle. \quad (3.21)$$

If we then calculate the linear-with- $k$  varying dipole moment of these Bloch functions, we can recognize the contribution coming from the second term in the  $c$  expansion together with the first term in the  $e$  expansion as the previously discussed contribution. We can, however, also combine the first term in the  $c$  expansion with the second in the  $e$  expansion. If we single out this contribution to  $d_z(\mathbf{k})$  we get

$$d_z(\mathbf{k}) = i \sum_{\mathbf{n}, \alpha, \beta} c_\alpha^*(0) c_\beta(0) \mathbf{k} \cdot \mathbf{n} \langle \alpha(\mathbf{0}) | \hat{d}_z | \beta(\mathbf{n}) \rangle \quad (3.22)$$

$$= i \sum_{\mathbf{n}} d_z^0(\mathbf{n}) (c_x^*(0) c_z(0) k_x n_x^2 + c_y^*(0) c_z(0) k_y n_y^2) \quad (3.23)$$

$$= \sum_{\mathbf{n}} d_z^0(\mathbf{n}) (l_x(0) k_y n_y^2 - l_y(0) k_x n_x^2). \quad (3.24)$$

**[normalization!!]** These expressions show us that, together with  $H_{soc} = \lambda \mathbf{l} \cdot \boldsymbol{\sigma}$  and  $H_{isb} = eE_z d_z$ , an additional Rashba-like term will appear in the energy dispersion [maybe a little more explanation is warranted here].

With the understanding that one can find Rashba like dispersions, coming not from the usually considered purely relativistic, but also from electrostatic means, we can look at an example situation where this leads to a gigantic spin-splitting in a bulk material, namely Germanium Telluride (GeTe).

### 3.4 Overview: Germanium Telluride

The space group of GeTe is R3m (#160 in International Tables), with ferroelectric polarization along the threefold rotation  $z$ -axis caused by an off-centering of the central Te atom Rabe and Joannopoulos (1987) as displayed in Fig. 3.1-(a). The valence and conduction bands are formed mostly by  $s$  and  $p$  orbitals from Te and Ge, respectively. This, together with the large spin-splitting in the vicinity of the  $Z$  point Di Sante *et al.* (2013) as observed from the band-structure in Fig. 3.1-(b), lends it as a perfect test-case of the above described mechanisms. Moreover, since it's a bulk material, we can rule out the possibility that the relativistic Rashba effects results in a contribution from the existence of possible large potential gradients at a surface. The band structure, presents a distinct large linear spin splitting around the  $Z$  point, resembling the well known Rashba effect. Due to time reversal symmetry, no spin-splitting is only present observed along the  $Z - A$  and  $Z - U$  paths, not the  $Z - \Gamma$  path. The density of states (DOS), displayed in Fig. 3.1-(c), confirms the orbital character of the bands, aluded to earlier.

### 3.5 Band structure

The bands we will focus on most are the three topmost valence bands. As seen in Fig. 3.1-(a), these bands have the largest spin-splitting, giving already a hint that as shown above, the atomic SOC is an important part, since it's bigger on Te, where the orbitals comprising these bands originate from. If one were to fit the dispersion from the topmost valence band to the form of the Rashba Hamiltonian Rashba and Sheka (1959); Lifshitz *et al.* (1982),

$$\mathcal{H}_R = \alpha_R (\mathbf{k} \times \mathbf{E}) \cdot \boldsymbol{\sigma}, \quad \alpha_R = \frac{e\hbar^2}{2m^2c^2}, \quad (3.25)$$

it would result in an abnormally large  $\alpha_R \approx 30.7 \text{ eV}\text{\AA}$  Di Sante *et al.* (2013), while, as discussed before, a more realistic prefactor would be  $\alpha_R = 10^{-6} \text{ eV}$  in the purely relativistic case inside the vacuum. This is even more abnormal considering the fact that this is a bulk material, and that it is known that proper ferroelectrics have zero polarization in open boundary conditions because the depolarizing fields are not screened. Moreover, in the periodic boundary conditions utilized by DFT, the potential mimics short circuit boundary conditions Meyer and Vanderbilt (2001),  $\mathbf{E} = 0$ , which results in zero contribution from Eq. 3.25.

The last issue with the purely relativistic explanation, which has been confirmed experimentally Krempaský, *et al.* (2016), lies in the orientation of the spin polarization of the split bands. According to Eq. 3.25, they should all be lined up. However, as has been shown and will be confirmed by our results

below, the orientation depends on the character of the band, more specifically the value of the total angular momentum  $j$ .

Wannier representation allows us to elucidate the  $k$ -dependent electric dipole moment arising due to interference of the atomic orbitals on the neighboring sites Marzari *et al.* (2012). In order to obtain the effective Hamiltonian, we write the Bloch functions as linear combinations of the Wannier functions that describe the bands of interest:

$$\psi_{\mathbf{k}}(\mathbf{r}) = \sum_{\alpha, \mathbf{R}} c_{\alpha}(\mathbf{k}) w_{\alpha}(\mathbf{r} - \mathbf{R}) e^{i\mathbf{k}\cdot\mathbf{R}},$$

where the Wannier functions  $w_{\alpha}(r)$  are chosen to be real and  $\mathbf{R}$  denote the unit cell in which the orbital is centered.

In the case of GeTe the electric polarization is along the  $z$  direction, making it sufficient to focus on the corresponding dipole moment

$$d_z(\mathbf{k}) = e \sum_{\alpha, \beta, \mathbf{R}} A_{\alpha, \beta}(\mathbf{k}) e^{i\mathbf{k}\cdot\mathbf{R}} \mathcal{Z}_{\alpha, \beta}^{\mathbf{R}} \quad (3.26)$$

$$A_{\alpha, \beta}(\mathbf{k}) = c_{\alpha}^*(\mathbf{k}) c_{\beta}(\mathbf{k}) \quad (3.27)$$

$$\mathcal{Z}_{\alpha, \beta}^{\mathbf{R}} = \int d\mathbf{r} w_{\alpha}(\mathbf{r}) w_{\beta}(\mathbf{r} - \mathbf{R}) z. \quad (3.28)$$

Expanding each term around  $k_Z$ , and keeping contributions up to first order in  $\mathbf{k}^r = (k_Z - \mathbf{k})$ , one obtains

$$d_z(\mathbf{k}) = e \sum_{\alpha, \beta, \mathbf{R}} \left( A_{\alpha, \beta}(Z) + \mathbf{k}^r \frac{\partial A_{\alpha, \beta}(\mathbf{k})}{\partial \mathbf{k}} \Big|_{\mathbf{k}=Z} \right) \times \\ (1 + i\mathbf{k}^r \cdot \mathbf{R}) \mathcal{Z}_{\alpha, \beta}^{\mathbf{R}}. \quad (3.29)$$

The term that combines the first order variation of  $A_{\alpha, \beta}(\mathbf{k})$  with the zeroth order term from the exponent leads to a nonzero contribution only if  $w_{\alpha}, w_{\beta} = s, p_z$  in the same unit cell ( $\mathbf{R} = 0$ ). This is the charge asymmetry that comes from  $s-p_z$  hybridization and was previously considered in the context of giant spin splitting at surfaces in Refs. 19; 20 and for bulk perovskites in Ref. 6. The new terms that we consider here combine the zeroth and first order contributions to  $A_{\alpha, \beta}(\mathbf{k})$  with the first order  $i\mathbf{k}^r \cdot \mathbf{R}$  term. Using indices 1, 2, 3 to denote  $p_x, p_y, p_z$  Wannier functions one obtains the following relation between the Bloch function coefficients and the OAM:  $l_k(\mathbf{k}) = -i\epsilon_{ijk} A_{ij}$ .

Upon closer inspection of the overlap dipole,  $\mathcal{Z}_{\alpha, \beta}^{\mathbf{R}}$ , one concludes that for  $d_z$  to be nonzero, at least one of the orbitals  $\alpha, \beta$  needs to be the  $p_z$  orbital and the shift-vector  $\mathbf{R}$  has to have a component along the second orbital ( $p_x$  or  $p_y$ ). This is illustrated in Fig. 3.3(a). Filling this into Eq. (3.29) and summing over the nearest neighbor unit cells ( $\mathbf{R} = \pm 1$ ), we arrive at

$$d_z(\mathbf{k}) = 4e \left( l_x(Z) + \mathbf{k}^r \frac{\partial l_x(\mathbf{k})}{\partial \mathbf{k}} \Big|_{\mathbf{k}=Z} \right) k_y^r R_y \mathcal{Z}_{y, z}^{R_y} \\ - 4e \left( l_y(Z) + \mathbf{k}^r \frac{\partial l_y(\mathbf{k})}{\partial \mathbf{k}} \Big|_{\mathbf{k}=Z} \right) k_x^r R_x \mathcal{Z}_{x, z}^{R_x}. \quad (3.30)$$

The coupling of the electric dipole moment with an external electric field, or in the case of GeTe, with the electric polarization, leads to a contribution to the

Hamiltonian of the form:

$$\mathcal{H}_{OR} \propto \mathbf{l} \cdot (\mathbf{k} \times \mathbf{E}) \quad (3.31)$$

The terms with  $l_{x,y}(Z)$  lead to a linear  $k$ -dependence of the band energy if the atomic SOC partially unquenches the OAM. The second term leads to energy contribution, quadratic in  $k$ , but results in a linear variation of the OAM even in the absence of SOC. This linear variation of the OAM will then couple to  $\sigma$  [also referred to as spin angular momentum (SAM)] through the atomic SOC, leading to the linear spin splitting.

The energy dispersion close to the  $Z$  point can thus be modeled by

$$\epsilon(\mathbf{k}) = \epsilon(Z) + \lambda_{so} \mathbf{l} \cdot \boldsymbol{\sigma} + c_1 \mathbf{l} \cdot (\mathbf{k} \times \mathbf{E}) + c_2 l_z^2, \quad (3.32)$$

where  $\epsilon(Z)$  contains a constant band shift, while the term with  $\lambda$  is the atomic spin-orbit coupling, and the latter terms represent the contribution due to the threefold symmetric crystal field for  $l = 1$ . To explicitly show how the linear variation of the OAM arises from the terms in Eq. (3.30), we performed a  $k \cdot p$ -expansion of the first valence band which leads to following expressions for the OAM around  $k = Z$ :

$$\begin{aligned} l_x &= -\frac{\lambda_{so}\sigma_x - c_1 E_z k_y}{c_2} \\ l_y &= -\frac{\lambda_{so}\sigma_y + c_1 E_z k_x}{c_2}, \end{aligned} \quad (3.33)$$

where we only included terms with the  $E_z$  component.

## 3.6 Methods

To back up this qualitative analysis, we performed quantitative ab initio calculations to study how the discussed effects manifest themselves in GeTe. Since we are interested in understanding the mechanism on a microscopic level, we use a tight-binding formalism based on Wannier functions Marzari *et al.* (2012). The gauge freedom during the Wannierization can then be exploited to provide a set of basis functions which are localized and resemble closely the atomic orbitals (spherical harmonics). To this end we first performed a nonrelativistic DFT calculation using the Quantum-Espresso package Giannozzi *et al.* (2009). We used 10x10x10 and 12x12x12 Monkhorst-Pack grids for sampling the reciprocal space in the self-consistent density and non-self-consistent calculations respectively, as well as an energy convergence threshold of  $10^{-8}$  Ry in both calculations. We used ONCVPSP pseudopotentials. The energy and density cutoffs were set to 56 Ry and 500 Ry respectively.

We then employed the Wannier90 software Mostofi *et al.* (2014) to perform the Wannier interpolation of the bands close to the Fermi level, using projections onto s and p orbitals of both the Ge and Te ions. Only the projective step in the Wannierization was used to obtain Wannier functions that have the symmetry of the initial projections and therefore resemble the atomic orbitals as closely as possible. This nonetheless resulted in adequately localized Wannier functions with a total spread of 21.12 Å<sup>2</sup>. The Wannier functions can then be exploited to compute how the observables of interest evolve as we progress through the Brillouin zone (BZ). There is, however, one last hurdle

to overcome. We are interested in relativistic effects, therefore SOC has to be accounted for. Since at present Wannier90 can not output the Wannier functions from fully-relativistic DFT calculations, we applied the atomic SOC by adding  $\lambda_{so}\mathbf{l} \cdot \boldsymbol{\sigma}$  term to the Wannier tight-binding Hamiltonian obtained from a collinear calculation. The matrix elements of  $\mathbf{l}$  operator were computed from the Wannier functions from the collinear calculation.  $\lambda_{so}$  parameters were fitted to reproduce the band structure from a relativistic DFT calculation, resulting in  $\lambda_{so}^{Te} = 0.33$ ,  $\lambda_{so}^{Ge} = -0.07$  eV. We only include SOC terms between Wannier functions that are centered at the same atom. This is referred to as the atomic centered approximation.

### 3.7 Results and Discussion

Focusing on the topmost valence band, displayed in the left panel of Fig. 3.4, there are several features that warrant a discussion. The first is that we clearly see the linear variation of the OAM even without SOC, with forms given by Eq. (3.33). Secondly, since only  $k_y$  varies along the  $A \rightarrow Z$  path, it is evident that the OAM along the  $y$  axis ( $l_y$ ) vanishes along the entire path. It is only when  $k_x$  varies, as the wavevector progresses along the  $Z \rightarrow U$  path, that we observe a nonvanishing  $l_y$ . Along this path, the sign of  $k_x$  is negative whereas the sign of  $k_y$  is positive just as along the  $Z - A$  path. This results in a consistent orientation of  $l_y$  and  $l_x$ , given by Eq. (3.33). The third observation is that including atomic SOC is manifested in the "unquenching" of the OAM. In Fig. 3.4, as soon as there is an infinitesimal variation of the the wave vector from the time-reversal invariant  $Z$ -point (where  $\mathbf{l} = 0$  due to the symmetry), the unquenching of OAM leads to a nonzero shift in the OAM, with the sign depending on the subband.

Lastly, to correlate the changes in the OAM and the dipole of the Bloch function, we computed the  $z$  coordinate of the center of mass  $\bar{z} = \int_{\text{supercell}} z|\psi(\mathbf{k})|^2$ , which is proportional to the dipole moment computed around the same reference point. Figure 3.4 shows the correlation of the dipole and OAM of the bands, consistent with Eq. (3.30), while Fig. 3.5 displays the asymmetric variation of the charge density of the first valence band along the  $Z \rightarrow A$  path. More specifically, there is a clear development of a nonzero dipole moment around Ge, which couples to the local  $E_z$ . These considerations also hold true for the third valence band, as seen from the right panel of Fig. 3.4.

In addition to the magnitude of  $\alpha_R$ , other important features are dependent on the orbital character of the bands, unlike in the case of the relativistic Rashba effect, as was discussed above. We see that for states with predominant  $j = \frac{3}{2}$  or  $j = \frac{1}{2}$  character, the SAM is oriented along or opposite to the OAM, respectively. Comparing the orientations of the SAM and OAM, shown in Fig. 3.6, we conclude that close to the  $Z$ -point, the topmost valence band has mostly  $j = \frac{3}{2}$  character, whereas the third mostly  $j = \frac{1}{2}$ . Interestingly, the states in the upper third valence band and lower first valence band switch characters when moving further away from the  $Z$  point, as seen in the panels (c) and (f) of Fig. 3.6. This draws attention to the fact that inclusion of Eq. (3.31) breaks threefold symmetry and results in  $j$  not being a good quantum number anymore. This causes a highly nontrivial SAM and OAM texture to be present in these two subbands, with both SAM and OAM varying considerably throughout the BZ.

When comparing the spin splitting of the two valence bands, their relative signs are opposite, an effect which cannot be explained by the relativistic Rashba effect [Eq. (3.25)], that leads to the same splittings, regardless of the character of the band. Only terms such as Eq. (3.30) can explain this behavior.

### 3.8 Conclusions

We have explored the microscopic origin of the giant Rashba-like spin splitting in the band structure of bulk ferroelectric GeTe with high atomic SOC. We derived the form of the band dispersion in the Wannier representation, that relates the large spin splitting to the intricate interplay between OAM, atomic SOC, the crystal field and the electric polarization. It turns out that the crucial component, which is not present in the relativistic Rashba effect, is the emergence of a nonzero electric dipole of the Bloch functions due to their OAM. The quantitative analysis based on Wannier functions and atomic-centered approximation confirms this mechanism in GeTe. We find a very good agreement between the proposed band dispersion, Eq. (3.32), and the dispersions of the first and third valence bands, where the effect manifests itself most clearly.

Ultimately, the results suggest that (1) large ferroelectric polarization, (2) high atomic SOC, and (3) highly symmetric environment producing little OAM quenching could be the design rules for new materials with strong Rashba-like spin splitting. These materials could enable spintronic devices with the much needed electric control of spin polarization.

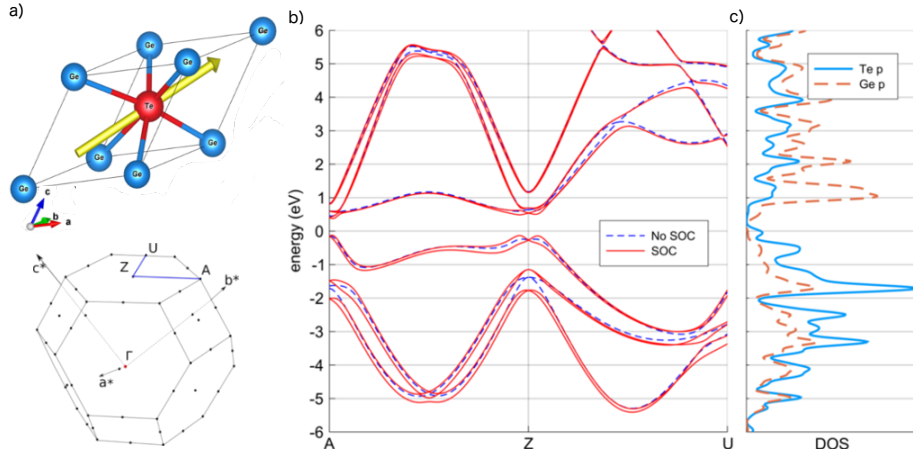


Figure 3.1: (a) Rhombohedral unit cell and Brillouin zone of GeTe, with the polarization direction in yellow. (b) Band structure obtained from a DFT calculation with and without SOC, along the blue path in panel (a). (c) partial DOS for Te and Ge p orbitals computed without SOC.

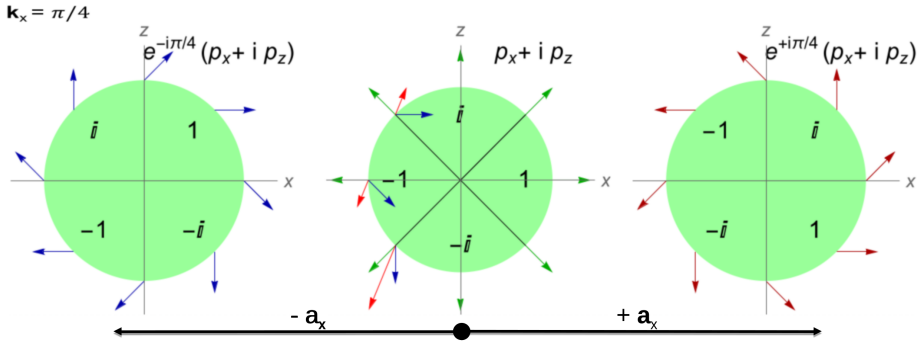


Figure 3.2: Interference between orbitals with nonzero OAM. Three neighboring unit cells are displayed, each with the same  $p_x + i p_z$  orbital (thus having nonzero  $l_y$ ). The wave functions of the left and right unit cells have their phase rotated by the plane-wave part  $e^{ik_x R_x}$ . The amplitude and phase of the wave function are encoded with the length and polar angle of the arrows.

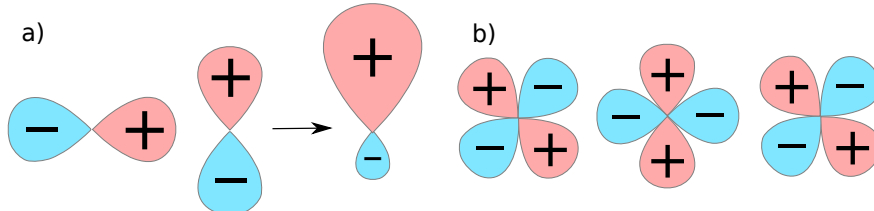


Figure 3.3: Overlap dipoles of orbitals in neighboring unit cells. (a) Nonzero dipole coming from shifted  $p$  orbitals. (b) Dipoles of shifted  $d$  orbitals compensate at a high symmetry point.

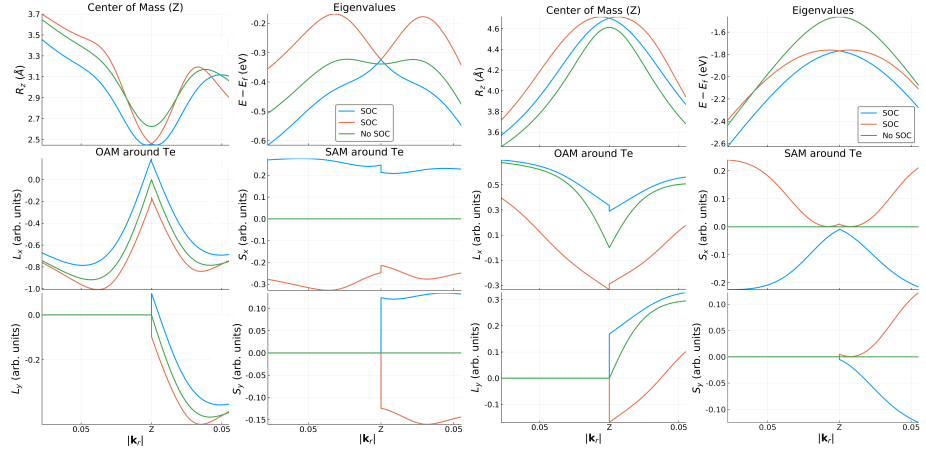


Figure 3.4: Comparison between the real-space observables and energy dispersion in (a) the first and (b) third valence band. The values are plotted in function of the relative distance from the  $Z$  point  $\mathbf{k}_r = \mathbf{k} - \mathbf{k}_Z$ , towards the  $A$  and  $U$  points. The green graphs denote the values before turning on atomic SOC, whereas the orange and blue graphs denote the two spin-split bands.

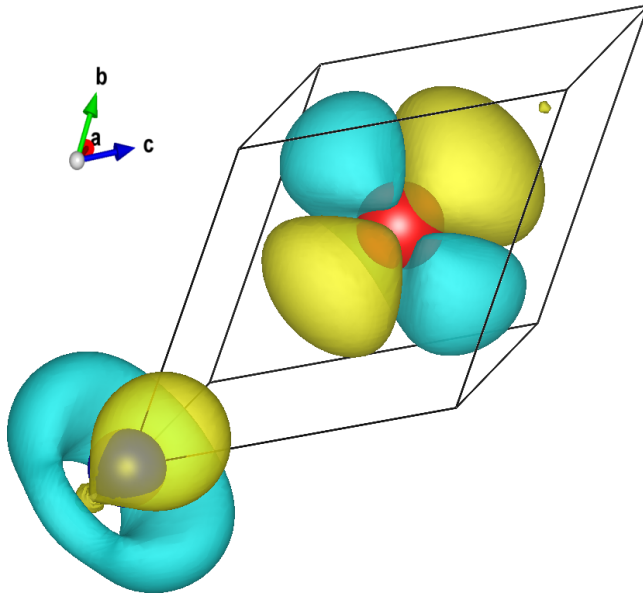


Figure 3.5: The variation of the charge density of the Bloch function of the first valence band  $\frac{\partial |\psi(\mathbf{k})|^2}{\partial \mathbf{k}} \Big|_{\mathbf{k}=\mathbf{Z}}$  away from  $Z$  towards  $A$ . Te and Ge ions are in red and blue, respectively. The charge asymmetry around Ge showcases the nonzero dipole moment along  $z$ , which couples to the local electric field near Ge ion.

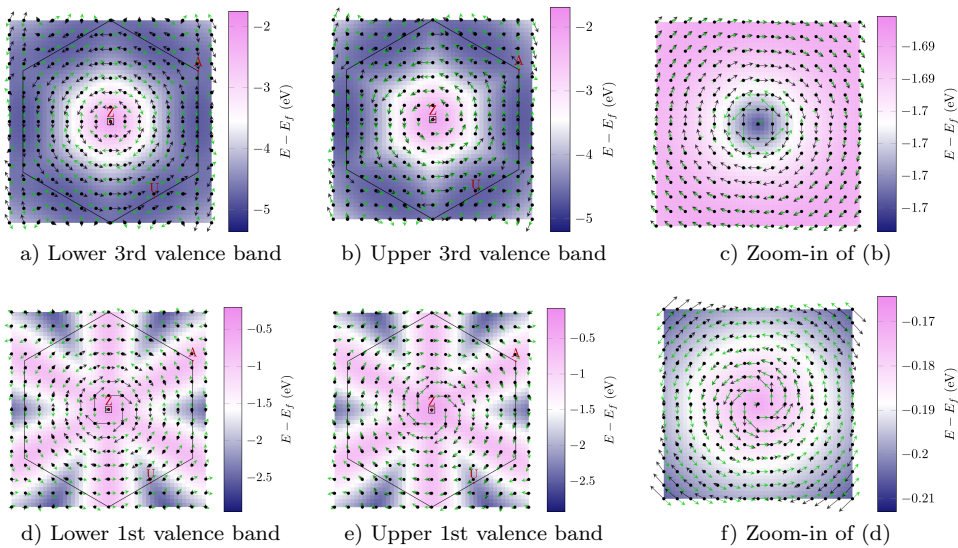


Figure 3.6: OAM and SAM textures around the  $Z$  point in the first and third valence bands of GeTe. The black and green arrows show the OAM and SAM textures, respectively. The length of the arrows was chosen separately for clarity in each figure and should thus not be compared. The color maps signify the energy of the bands, relative to the Fermi level. The small box around the  $Z$  point indicates the area, magnified in panels (c) and (f). In the zoomed figures (c) and (f) one can observe the change or relative orientation between the SAM and OAM when moving away from the  $Z$  point, signifying a change of character between  $j = 1/2$  and  $j = 3/2$ .



# Bibliography

- S. Datta and B. Das, Applied Physics Letters **56**, 665 (1990).
- A. D. Kent and D. C. Worledge, Nature Nanotechnology **10**, 187 (2015).
- T. Jungwirth, X. Marti, P. Wadley, and J. Wunderlich, Nature Nanotechnology **11**, 231 (2016).
- D. Di Sante, P. Barone, R. Bertacco, and S. Picozzi, Advanced Materials **25**, 509 (2013).
- K. Ishizaka, Nature materials **10**, 521 (2011).
- M. Kim, J. Im, A. J. Freeman, J. Ihm, and H. Jin, Proceedings of the National Academy of Sciences of the United States of America **111**, 6900 (2014).
- M. Liebmann, C. Rinaldi, D. Di Sante, J. Kellner, C. Pauly, R. N. Wang, J. E. Boschker, A. Giussani, S. Bertoli, M. Cantoni, L. Baldrati, M. Asa, I. Vobornik, G. Panaccione, D. Marchenko, J. Sánchez-Barriga, O. Rader, R. Calarco, S. Picozzi, R. Bertacco, M. Morgenstern *et al.*, Advanced Materials **28**, 560 (2016).
- J. Krempaský, H. Volfová, S. Muff, N. Pilet, G. Landolt, M. Radović, M. Shi, D. Kriegner, V. Holý, J. Braun, H. Ebert, F. Bisti, V. A. Rogalev, V. N. Strokov, G. Springholz, J. Minár, J. H. Dil, Phys. Rev. B **94**, 205111 (2016)
- .
- E. Rashba and V. Sheka, New. J. Phys. **17**, 050202 (2015).
- E. M. Lifshitz, V. B. Berestetskii, and L. P. Pitaevskii, *Course of Theoretical Physics - Volume 4: Relativistic Quantum Theory*, 2nd ed. (Elsevier, Oxford, 1982).
- K. M. Rabe and J. D. Joannopoulos, Phys. Rev. B **36**, 6631 (1987).
- K. F. Garrity, K. M. Rabe, and D. Vanderbilt, Phys. Rev. Lett. **112**, 127601 (2014).
- B. Meyer and D. Vanderbilt, Phys. Rev. B **63**, 205426 (2001).
- S. R. Park, C. H. Kim, J. Yu, J. H. Han, and C. Kim, Phys. Rev. Lett. **107**, 156803 (2011).
- J. H. Park, C. H. Kim, J. W. Rhim, and J. H. Han, Phys. Rev. B **85**, 195401 (2012).

- S. R. Park and C. Kim, J. Electron. Spectros. Relat. Phenomena **201**, 6 (2015).
- J. Hong, J.-W. Rhim, C. Kim, S. Ryong Park, and J. Hoon Shim, Sci. Rep. **5**, 13488 (2015).
- N. Marzari, A. A. Mostofi, J. R. Yates, I. Souza, and D. Vanderbilt, Rev. Mod. Phys. **84**, 1419 (2012).
- L. Petersen and P. Hedegård, Surf. Sci. **459**, 49 (2000).
- D. Go, J.-P. Hanke, P. M. Buhl, F. Freimuth, G. Bihlmayer, H.-W. Lee, Y. Mokrousov, and S. Blügel, Sci. Rep. **7**, 46742 (2017).
- P. Giannozzi, *et al.* J. Phys.: Cond. Mat. **21**, 395502 (2009).
- A. A. Mostofi, J. R. Yates, G. Pizzi, Y. S. Lee, I. Souza, D. Vanderbilt, and N. Marzari, Comp. Phys. Comm. **185**, 2309 (2014).